Journal of Engineering Science and Technology
Vol. 15, No. 3 (2020) 1506 - 1519
© School of Engineering, Taylor's University

CRYSTALLITE SIZES ON THE PHOTOCATALYTIC PERFORMANCE OF SUBMICRON WO_3 PARTICLES

ASEP BAYU DANI NANDIYANTO*, RISTI RAGADHITA, ROSI OKTIANI, AJENG SUKMAFITRI, MELI FIANDINI

Departemen Pendidikan Kimia, Fakultas Pendidikan Matematika dan Ilmu Pengetahuan Alam, Universitas Pendidikan Indonesia, Dr. Setiabudi no 229, Bandung 40154, Jawa Barat, Indonesia
*Corresponding author: nandiyanto@upi.edu

Abstract

Strategies on designing optimum photocatalyst materials have attracted tremendous attention. One of the most important designing parameters is crystallite size. However, the effect of this parameter on photocatalytic performance is still not fully understood. Some reports confirmed positive impacts, while the others showed the opposite results. The main reason for the uncompromised reports is due to the inconsideration of interfering other parameters during the photocatalytic process, such as excessive surface area, quantum effect, and change structure in the catalyst such as porosity. This report evaluates correlations between crystallite sizes and photocatalytic performance of submicron photocatalyst particles. Experiments used submicron tungsten trioxide (WO_3) as a model of catalyst for degrading curcumin in the batch photoreactor system. To ensure the evaluation precisely, this study makes the photocatalytic process to be restricting the reaction occurring on the surface of catalyst only. To achieve this condition, submicron dense WO_3 particles were used and produced from pure ammonium tungstate pentahydrate with no additional chemicals, solvents, surfactants, and additives using a sequential ball-milling and crystallization route. Experimental results showed that the photocatalytic performance was strongly dependent on the crystallite sizes, in which it improved with the use of larger crystallite sizes. The impact of crystallite sizes was verified by testing the process using various catalyst particle outer diameters (from 200 to 1200 μm) and compositions of catalyst/curcumin. The catalytic rate is directly proportional to the crystallite size; in general, the improvement of the rate would be double when doubling the crystallite size. The proposal of the fundamental consideration was also added for explaining the phenomena in the photocatalytic process. Because the optimization of this crystallite size parameter offers essential information for practical applications, the results of this study are important and relevant to other functional catalytic properties.

Keywords: Crystallite size, Curcumin, Photodecomposition rate, Submicron particles, Tungstate material.

1. Introduction

Reports on the obtainment of the excellent photocatalytic process have been well-documented, involving several parameters:

(i) types of materials [1-6];
(ii) process condition, such as temperature, pH, radiation intensity, illumination time, [1, 4, 7, 8] as well as a ratio between catalyst and reactant [4, 9] and its solubility in an aqueous solvent;
(iii) size, morphology, and surface chemistry of catalyst [10-12];
(iv) crystallinity as well as crystallite size and structure [10, 13, 14];
(v) existence of doped material and co-catalyst [1-3, 6, 15].

One of the most important parameters is the crystallite size. However, correlations between crystallite sizes and photocatalytic performance are still not fully understood. Some papers confirmed positive impacts [16, 17] while the others showed the opposite results [5, 18] since it cannot be predicted [19]. The main reason for the uncompromised reports is due to interfering other parameters during the photocatalytic process. For example, when utilizing nanoparticles as instruments for examining photocatalytic parameters, they sometimes get misrepresentative information since they have issues regarding quantum confinement effects and over dominance in the surface area [19, 20]. The utilization of film-typed catalyst [17, 18, 21] has shortcomings, such as (i) the embedded catalyst in the specific position, (ii) issues on inadequacy of light penetration, (iii) interaction between reactant and catalyst, and (iv) existence of attached impurities on the catalyst (that cannot be repealed easily, making blockage for further catalytic processes) [12].

Previously, we reported strategies for the preparation of photocatalyst particles with controllable morphologies (including outer diameters, shapes, and porosity) and crystallinity [6, 7, 10, 12-15, 22, 23], in which these were aimed for gaining excellent photocatalytic performance only. Our previous studies did not give attention in detail on the crystallite size parameter, specifically when evaluating catalyst particles with sizes in the submicron range while this type of particles is typically disregarded and rarely reported. In fact, submicron catalyst brings exceptional results, which are different significantly from those of nanoparticles, film-typed materials, or bulk forms.

Submicron catalyst is easily mix, fly, and sink in the suspension during the photocatalytic process. This is different from film-typed catalysts that have issues in the fixed catalyst position, light penetration, as well as the number of reactant-catalyst contact and interaction [14]. Different from nanoparticles, submicron particles are spontaneously precipitated and settled. Indeed, this makes them easily collected (after the catalytic process) [24] and gives advantages in the characterized sample to be uncontaminated (getting the precise photocatalytic measurement). Further, compared to nanoparticles, the submicron particles' photocatalytic rate is slower, giving benefits for better distinguishing the deviation results.

The objective of this study was to systematically evaluate the impact of crystallite sizes on the photocatalytic performance of submicron particles. Experiments were conducted by evaluating the performance from submicron monoclinic tungsten trioxide (WO_3) as a model of catalyst for degrading curcumin in the batch photoreactor system.

WO_3 was selected as a model photocatalyst because it has excellent performance, such as chemical and thermal stable, active under visible light, and good photostability [22]. Various phases of WO_3 exist (e.g., orthorhombic, tetragonal, triclinic, monoclinic, and hexagonal) [14], and the present study used monoclinic phase because it is the most active and the most stable crystalline phase [9].

In the experimental procedures, submicron WO_3 particles with controllable particle outer diameters (from 200 to 1200 μm) and crystallinities (amorphous and crystalline with crystallite sizes from 0 to 20 nm) were produced from pure ammonium tungstate pentahydrate (ATP) using a sequential ball-milling and crystallization route. In general, the ball-milling process was used for controlling particle outer diameters, and the crystallization route was for controlling crystallite sizes by changing heating temperature. The present method did not involve additional chemicals, additives, and solvents during the preparation procedure to ensure the precise evaluation in the photocatalytic process. The existence of chemicals, additives, and solvents may trigger the formation of unique structure (such as pores) in the final product [22, 23, 25], which in turn changes the photocatalytic reaction and gives misleading in the measurement for getting the singular impact of crystallite size.

The impact of crystallite sizes also confirmed by testing the photocatalytic process using various particle outer diameters and composition ratios of catalyst and reactant (i.e., curcumin). The proposal of fundamental consideration was also added to complete the explanation of the phenomena happening during the photocatalytic process.

2. Experimental Method

Materials

This study used ATP (>99%; $(NH_4)_{10}[W_{12}O_{41}]$. 5 H_2O; Kanto Chemical Co., Inc., Japan) as a tungstate-related raw material and curcumin solution (obtained by extracting local turmeric (Curcuma longa L); purchased from a local market in Bandung, West Java, Indonesia; see our previous studies [7]) as a dye model. Prior to the process, ATP was preheated at a temperature of 100°C for 30 minutes to remove physically adsorbed water.

In short, for the production of WO_3 particles, the experimental procedure involved the immediate steps sequentially: (i) ball-milling process, and (ii) crystallization process. No additional solvent, chemical, or additive during the synthesis of WO_3 particles from ATP.

Ball-milling process

The preheated ATP was put into the ball-milling apparatus that consisted of cylinder stainless steel milling vial (length = 7 cm; inner diameter = 14 cm) and 8-mm stainless steel balls, in which detailed information for the ball-milling apparatus is presented in the literature [26, 27]. The milling process condition was fixed and performed using a rotation speed of 100 rpm and the working volume of 30% at room temperature and atmospheric condition. In this study, the ball-to-ATP mass ratio was varied from 40 to 160, depending on the desired final particle outer diameter.

Crystallization

4 grams of the ball-milled ATP powder with a specific mean outer diameter was put into an electric furnace. The crystallization was done at a specific heating temperature, varied from 100 to 800°C. To ensure the crystallization process, the sample was directly put into the furnace at a specific temperature for 30 minutes and cooled to room temperature (with cooling rate = 30°C/min).

Characterizations

Several characterizations were conducted:

(i) Thermal Analysis (TG/DTA; DTG-60A, Shimadzu Corp., Japan) for analyzing the thermal properties of ATP.

(ii) X-ray powder diffraction (XRD; PANalytical X'Pert PRO; Philips Corp., The Netherlands) and Fourier Transform Infrared Spectroscopy (FTIR; FTIR-4600, Jasco Corp., Japan) for analyzing the crystal phase/pattern and the chemical composition, respectively. To get crystallite size based on the XRD results, a calculation using a Scherer analysis was adopted.

(iii) Scanning Electron Microscope (SEM; SEM, JSM-6360 LA; JEOL Ltd., Japan) for analyzing the particle morphology. The particle outer diameters were measured using a Ferret analysis of more than 100 individual particles in SEM images.

(iv) The nitrogen adsorption/desorption analysis (Nova 4200e; Quantachrome Instruments Corp., US) for analyzing the porosity and surface area of the sample.

In the photocatalytic measurement, the prepared submicron WO_3 particles were put into the batch-typed photocatalytic apparatus for degrading curcumin solution. The photocatalytic apparatus consisted of a borosilicate batch glass reactor (inner diameter = 8 cm and height = 10 cm), light sources (36 W of Neon Lamps), a bubbler (for introducing air (1 L/min)), and a magnetic stirrer (600 rpm). Prior to conducting photocatalytic experiments, each process was initiated by mixing and allowing the WO_3-curcumin suspension to equilibrate for 5 minutes without adding any light irradiation.

The photocatalytic experiments were done at room temperature and atmospheric condition for 120 minutes, and the progress of the photodegradation was observed by taking out a definite quantity of sample, which were then directly analyzed using a visible spectrophotometer (Model 7205 JENWAY; Cole-Parmer; US) for obtaining absorbance results.

The absorbance results were subsequently normalized, and the maximum peak was put into the calculation based on Beer's Law to obtain the concentration of curcumin [7]. To calculate the photocatalytic rate empirically, the Langmuir–Hinshelwood kinetic model was used using the following expression [22]:

$$-\frac{dC}{dt}=\frac{k_T.K_C.C}{1+K_C.C} \quad (1)$$

where C is the concentration of curcumin at a specific time, and k_T is the apparent photoreaction rate constant. K_C is the apparent equilibrium constant for adsorbing reactants (such as curcumin) on the photocatalyst surface, in which it relates to the concentration of chemical species, such as oxygen (O_2), water (H_2O), and hydroxide

(OH^-) [28]. Assuming the process is done under constant catalyst amount and very low concentration of the reactant (concentration of curcumin = less than 100 ppm), we can get the expression model as [22]:

$$-\frac{dC}{dt} = k.C \tag{2}$$

where k is the photoreaction constant, which is derived from $k = k_T.K_C$. The value of k is then used in this study to confirm the photocatalytic rate.

3. Results and Discussion

Figures 1(a) to (d) depict the SEM images of the prepared WO_3 particles with various crystallite sizes and outer diameters. The results showed that additional ball-milling process could create the particles with outer diameters from sub-micrometer to several micrometers without changing chemical structure, and crystallization process has the impact on controlling crystallite size.

FTIR (Fig. 1(e)) and XRD (Fig. 1(f)) present different peaks and patterns for WO_3 with various crystallite sizes, in which this is due to the fact that varying the crystallization temperature is effective in giving impact on converting ATP into WO_3 and controlling crystallite sizes. These results are in line with the TG/DTA results (Fig. 2). The TG/DTA analysis showed the decreases in the mass during the calcination, involving some exothermic and endothermic reactions for the conversion of ATP into WO_3 material [29].

The changes in the FTIR peaks and patterns were detected (Figure 1(e)), which is due to the change of chemical structure in the sample as the effect of temperature [29]. The main disappeared peaks were at wavenumber of about 1400 and 3000 cm^{-1}, corresponding to the NH- and OH-related components, respectively [30]. Existence of these peaks in the samples heated at 235°C indicates the presence of remained ammonia and water residue in the sample [13]. Indeed, these peaks are completely disappeared when heating at higher temperatures. The results also confirmed that when adding crystallization process at higher than 235°C to the ball-milled sample, ATP converts into WO_3 [14]. These results are in a good agreement with the TG-DTA analysis in Fig. 2.

Changes in the XRD peaks and patterns were identified for all cases (Figure 1(f)). Heating ATP at temperature of 150°C results no change in the XRD peaks and patterns (not displayed). Then, adding crystallization temperature of 235°C resulted in the production of amorphous-structured material [13]. Applying crystallization at temperatures of more than 300°C resulted in the appearance of XRD peaks (not displayed). Then, further increases in the temperature were followed by the increases in the XRD peak intensities [14]. All XRD peaks and patterns for all cases are identical to the standard the joint committee for the powder diffraction system (JCPDS) no. 72–1465 for monoclinic WO_3 [14]. No impurity peaks and no transition to other phases were identified, indicating that the heated ATP results in pure WO_3 in both chemistry and crystalline phase. The peak intensities seem to get the impact from the change of temperature. The larger particles have stronger signal for peak intensity than the smaller particles. The Scherer analysis showed that the increases in the crystallization temperature changed the crystallite size. Detailed effect of temperature on the crystallite size is shown in Fig. 3.

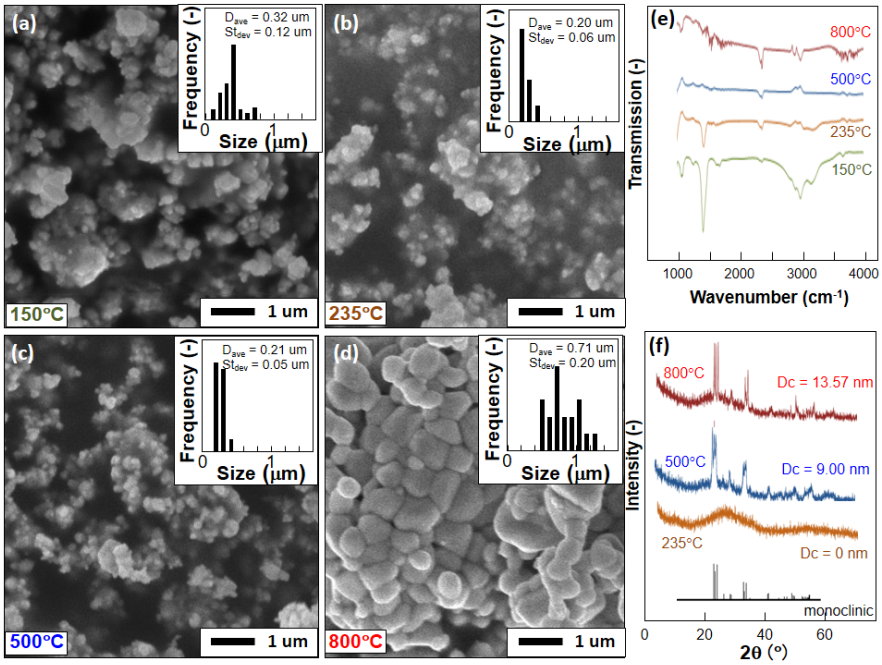

Fig. 1. The SEM (a-d), the FTIR (e), and the XRD (f) analysis results of the ball-milled ATP heated at various temperatures. Figs. (a), (b), (c), and (d) are ball-milled ATP heated at 150, 235, 500, and 800˚C, respectively. *Dp* is the particle outer diameter, and *Dc* is the crystallite size.

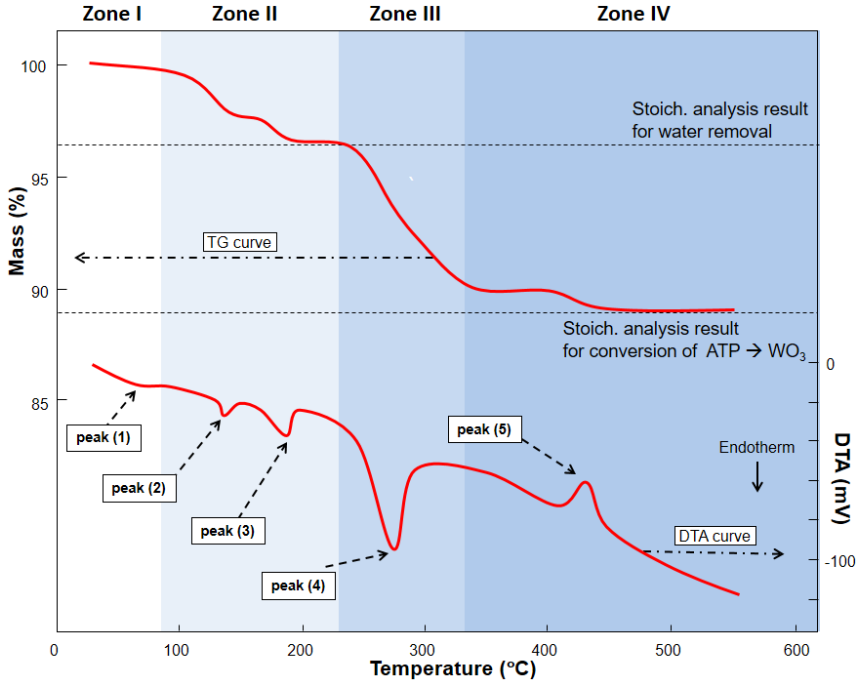

Fig. 2. TG/DTA of the ATP sample.

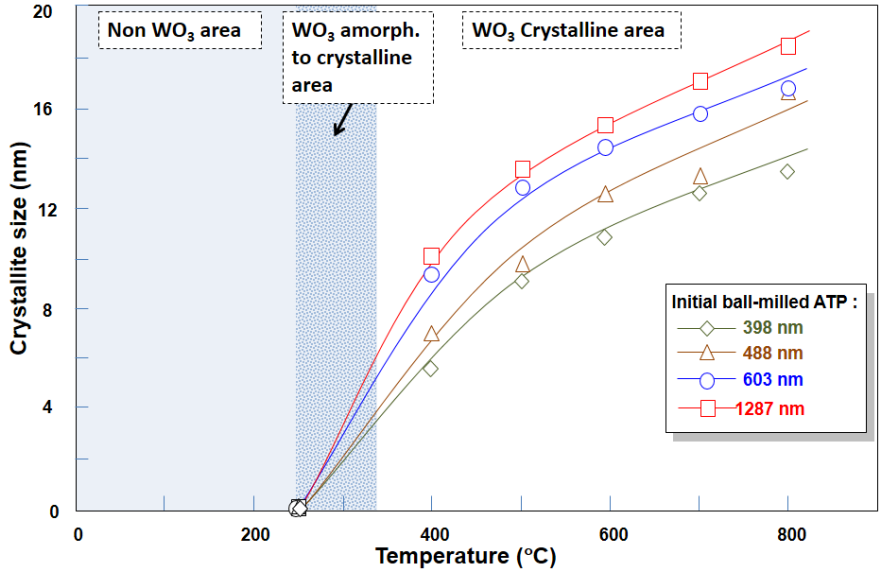

Fig. 3. Correlation between crystallite size and crystallization temperature for samples with various sizes.

Figure 4 presents the nitrogen sorption analysis results of the prepared WO_3 particles with various outer diameters and crystal sizes. To make easier distinguishing the results, different colors were applied for each sample. Different curves for the adsorption and desorption were obtained. The gap between adsorption and desorption lines for smaller particles is broader than that for larger particles, informing the larger surface area for the smaller particles. Different maximum volume adsorbed values were found, but they are less than 75 cc/g (relatively small compared to porous material [25]). All samples have nitrogen sorption characteristics of dense material without mesopore structures [31], confirmed by pore radiuses of less than 7 nm. The pores were relatively inactive for photoreaction since this pore size range (less than 7 nm) has limitations in the light penetration as well as chemical and oxygen diffusion into the deepest active sites in the pores [12]. Thus, the photocatalytic process is conducted only on the outer surface of the photocatalyst particle. The formation of dense particles without mesopores structure is due to the use of direct heat treatment of ATP without additional additives, chemicals, surfactants, or solvent to produce WO_3 particles [13, 14]. The analysis of surface area also confirmed that smaller-sized particles have larger surface area, and crystallite sizes have no impact on the change in the surface area (see Table 1 for comparison surface area).

Photocatalytic experiments using 30-ppm curcumin showed that the absorbance decreased over reaction time, informing the degradation of curcumin (Fig. 5). Converting the absorbance using Beer's law, the concentration of curcumin can be obtained [7]. 120-minute photodegradation process is a sufficient photocatalytic time to determine the differences in the catalytic rates. The photoreaction rate constants calculated using the above equation (2) are also paneled in Fig. 5.

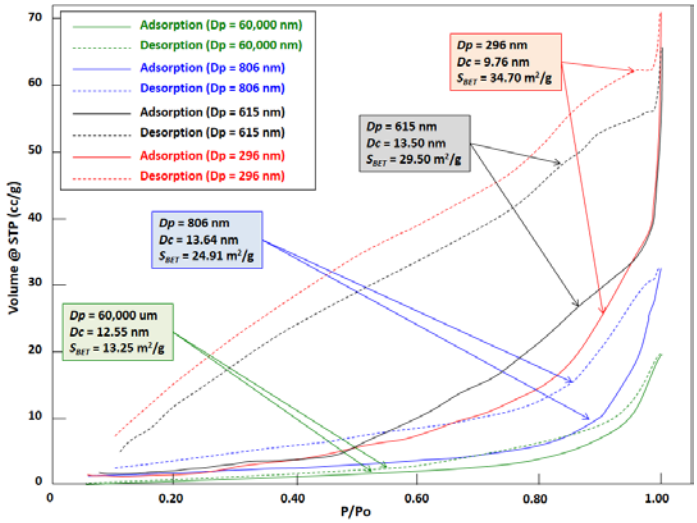

Fig. 4. Nitrogen adsorption/desorption analysis results of submicron WO_3 particles with various crystallite sizes and outer diameters. *Dp* is the particle outer diameter, *Dc* is the crystallite size, S_{BET} is the surface area using BET analysis.

The concentration of illuminated curcumin with no additional WO_3 catalyst (blank test) resulted in insignificant decomposition (final curcumin concentration of 98%) (see dotted and dashed line). The slight decrease in the concentration was found when using 60-um WO_3 catalyst particles, and the dramatic changes in concentration were found when using smaller catalysts, confirming that the main reason for the decomposition of curcumin is because of the existence of WO_3 as the photocatalyst [22]. The faster degradation rate was found for smaller catalyst, which were due to increases in the number of surface active area [10]. Further decreases in the concentrations were obtained when using catalysts with larger crystallite sizes (see dashed line). These results confirmed the important roles of the crystallite sizes on the improvement of catalytic performance, which are in a good correlation to other reports [16, 17]. Table 1 shows the comparison of particle outer diameter, surface area, and catalytic rate. The results confirmed that the crystallite size improved proportionally the catalytic rate.

Table 1. Correlation of particle outer diameter, crystallite size, surface area, and catalytic rate.

Particle outer diameter (nm)	Crystallite size (nm)	Surface area (m^2/g)	Catalytic rate (h^{-1})	Crystallite size ratio*	Catalytic rate ratio*
60,000	12.55	13.25	0.0204	-	-
60,000	19.12	14.15	0.0558	1.5235	2.7353
806	13.64	24.91	0.2701	-	-
834	18.56	23.96	0.3215	1.3607	1.1903
615	13.50	29.50	0.3718	-	-
296	9.76	34.70	0.4322	-	-
243	12.94	34.15	0.4846	1.3258	1.1212

Note: *ratio was obtained by comparing the larger crystallite size and the smaller crystallite size in the same particle outer diameter

The photodecomposition experiments using higher concentrations of curcumin were conducted (Fig. 6). The decomposition rate of 100-ppm curcumin (Fig. 6) is slower than that of 30-ppm curcumin (Fig. 5). The best absorption of curcumin was produced from materials with D_p of around 250 μm while the lowest absorption was caused by materials with D_p of around 60 μm. The higher amount of curcumin relates to the turbidity that prevents light transmission through the suspension [7]. Although there is an impact from color from the point of view light wavelength adsorption, this study focused on the decoloration of dye for analyzing the effect of crystallite size. Similar tendency in the effect of crystallite sizes on the enhancement of catalytic performance for degrading 30- and 100-ppm curcumin was found.

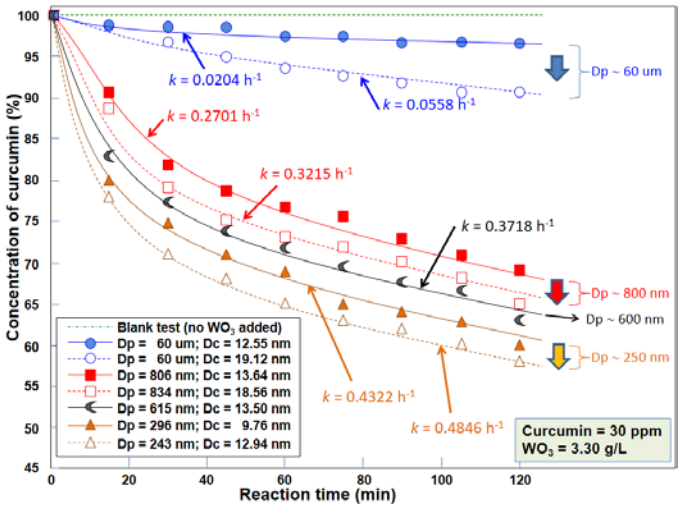

Fig. 5. Photodecomposition of 30-ppm curcumin using WO_3 particles with various crystallite sizes and outer diameters.

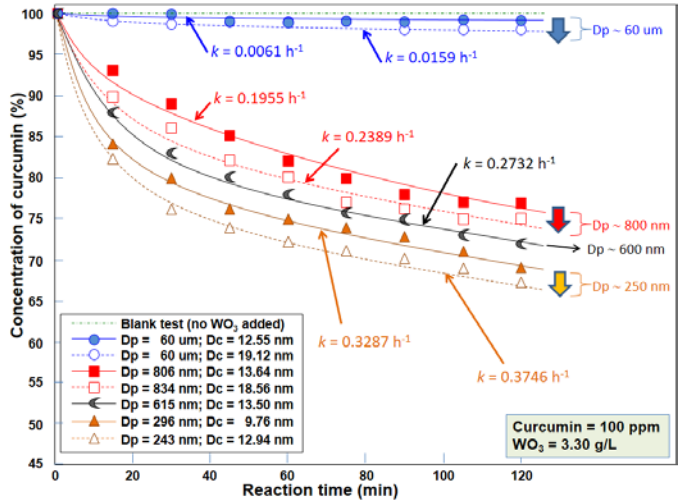

Fig. 6. Photodecomposition of 100-ppm curcumin using WO_3 particles with various crystallite sizes and outer diameters.

Figure 7 presents the calculated photocatalytic rate as a function of crystallite size under various outer catalyst particle diameters. All particle outer diameters agree that the improvement of photodecomposition rate depends on crystallite size.

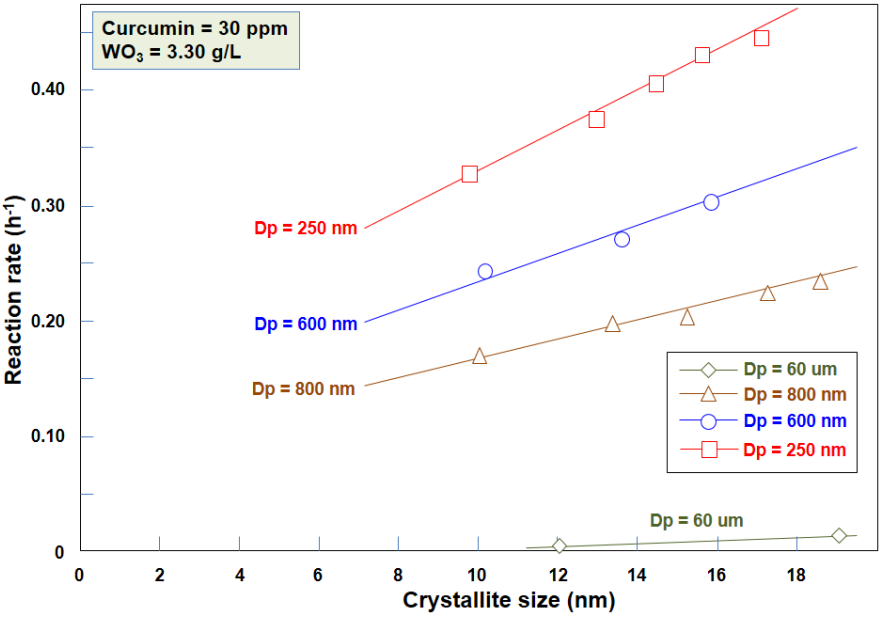

Fig. 7. Correlation between photodecomposition rate (30-ppm curcumin) and crystallite size under various particle outer diameter.

The illustration of the photocatalytic mechanism is presented in Fig. 8. Two bands (i.e., valence band (VB) and conduction band (CB)) plays an important role in the photocatalytic process. When catalyst absorbs photon as light energy (route P1), electron (e^-) moves from VB and migrate to CB (route P2) [11]. The promoting e^- releases hole (h^+) or an electron vacancy in the VB.

In general, the activation of e^- and h^+ (namely the photon-generated carriers) relates to the bandgap energy between CB and VB [21]. The successful activation of photon-generated carriers can be achieved when catalyst absorbs energy from photon that is equal to or higher value than catalyst's bandgap energy (bandgap of WO_3 = 2.98 eV) [6].

For some cases, e^- and h^+ can be recombined in the VB (see route P3). Once e- and h^+ separate (namely the charge separation), they become active. e^- travels to the photocatalyst surface (route P4) [8, 32]. The carriers accumulate on the photocatalyst surface, interacting with the adsorbed chemical species (such as oxygen (O_2), water (H_2O), and hydroxide (OH^-)) on the outer surface of photocatalyst, and participating in the reduction-oxidation reaction [11].

h^+ is active for converting the surface-bound H_2O or OH^- to hydroxyl radical (OH*) (route P5), whereas e^- takes electron-accepting species (i.e., O2) to form radical anions (such as superoxide (O_2*)) (route P4), endorsing the further conversion of other H_2O molecules into OH* (route P6) [5]. The existence of OH* permits the breaks apart of organic molecules into smaller organic components,

carbon dioxide, and water (route P7), confirmed by the appearance of bleaching color of curcumin in the photocatalytic process (Figs. 5 and 6).

The movement of photon-generated carrier depends on crystallite size [14], in which their diffusion time is simply explained as [13, 14]:

$$\tau = k_D \, r_{CZ}^2 / \pi D \tag{3}$$

where τ is the diffusion time, r_{CZ} is the crystallite size, and D is the diffusion coefficient of the photon-generated carrier [8]. k_D is the coefficient for interaction, relating to the efficiency of catalyst in absorbing a photon and the band gap energy. The above correlation shows that the larger crystallite creates advantages:

(i) The more adsorbed energy [20, 32].

(ii) The reduction of number in the recombination process (the re-position and the movement of photon-generated carriers to their originated state) [14, 17].

(iii) The faster travels of photon-generated carriers to reach the surface of the catalyst [8, 17].

(iv) The accumulation and increases in the number of the photon-generated carriers on the surface of the photocatalyst particle [17].

Above benefits give consequences on the more interaction with O_2, H_2O, and OH^-on the surface of photocatalyst [17, 19].

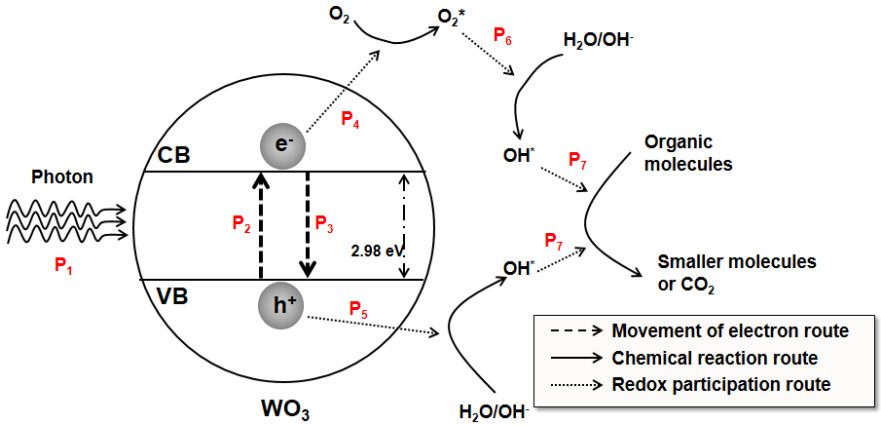

Fig. 8. Illustration of the phenomena happening during photocatalysis.

4. Conclusion

This study has investigated correlations of crystallite sizes and photocatalytic performance of submicron WO_3 particles, which is explained with the proposal of fundamental consideration for the phenomena happening during the photocatalytic process. Experimental results confirmed that the important role of crystallite sizes, in which the use of larger crystallite sizes has a direct impact to the improvement of photocatalytic performance, and this has been confirmed in the process using various outer catalyst diameters and compositions of catalyst/reactant. Because optimization of this crystallite size parameter brings crucial information for

practical applications, results in the importance of this study and their relevancies to other developments in the functional catalytic properties.

Acknowledgements

We acknowledged RISTEK BRIN for supporting this research (Grant-in-aid Penelitian Terapan Unggulan Perguruan Tinggi (PTUPT)).

References

1. Abdullah, A.M.; Al-Thani, N.J.; Tawbi, K.; and Al-Kandari, H. (2016). Carbon/nitrogen-doped TiO_2: New synthesis route, characterization and application for phenol degradation. *Arabian Journal of Chemistry*, 9(2), 229-237.
2. Badli, N.A.; Ali, R.; Bakar, W.A.W.A.; and Yuliati, L. (2017). Role of heterojunction ZrTiO4/ZrTi2O6/TiO2 photocatalyst towards the degradation of paraquat dichloride and optimization study by Box–Behnken design. *Arabian Journal of Chemistry*, 10(7), 935-943.
3. Nadarajan, R.; Bakar, W.A.W.A.; Ali, R.; and Ismail, R. (2018). Photocatalytic degradation of 1, 2-dichlorobenzene using immobilized TiO2/SnO2/WO3 photocatalyst under visible light: Application of response surface methodology. *Arabian Journal of Chemistry*, 11(1), 34-47.
4. Sakthivel, S.; Neppolian, B.; Shankar, M.; Arabindoo, B.; Palanichamy, M.; and Murugesan, V. (2003). Solar photocatalytic degradation of azo dye: Comparison of photocatalytic efficiency of ZnO and TiO2. *Solar Energy Materials and Solar Cells*, 77(1), 65-82.
5. Vamvasakis, I.; Georgaki, I.; Vernardou, D.; Kenanakis, G.; and Katsarakis, N. (2015). Synthesis of WO3 catalytic powders: evaluation of photocatalytic activity under NUV/visible light irradiation and alkaline reaction pH. *Journal of Sol-Gel Science and Technology*, 76(1), 120-128.
6. Arutanti, O.; Nandiyanto, A.B.D.; Ogi, T.; Iskandar, F.; Kim, T.O.; and Okuyama, K. (2014). Synthesis of composite WO3/TiO2 nanoparticles by flame-assisted spray pyrolysis and their photocatalytic activity. *Journal of Alloys and Compounds*, 591, 121-126.
7. Nandiyanto, A.B.D.; Sofiani, D.; Permatasari, N.; Sucahya, T.N.; Wiryani, A.S.; Purnamasari, A.; Rusli, A.; and Prima, E.C. (2016). Photodecomposition profile of organic material during the partial solar eclipse of 9 march 2016 and its correlation with organic material concentration and photocatalyst amount. *Indonesian Journal of Science and Technology*, 1(2), 132-155.
8. Zhang, L.; Wang, W.; Zhou, L.; and Xu, H. (2007). Bi2WO6 nano‐and microstructures: shape control and associated visible‐light‐driven photocatalytic activities. *Small*, 3(9), 1618-1625.
9. Szilágyi, I.M.; Madarász, J.; Pokol, G.r.; Király, P.; Tárkányi, G.; Saukko, S.; Mizsei, J.; Tóth, A.L.; Szabó, A.; and Varga-Josepovits, K. (2008). Stability and controlled composition of hexagonal WO3. *Chemistry of Materials*, 20(12), 4116-4125.
10. Arutanti, O.; Ogi, T.; Nandiyanto, A.B.D.; Iskandar, F.; and Okuyama, K. (2014). Controllable crystallite and particle sizes of WO3 particles prepared

by a spray ‐ pyrolysis method and their photocatalytic activity. *AIChE Journal*, 60(1), 41-49.

11. Nagaveni, K.; Hegde, M.; Ravishankar, N.; Subbanna, G.; and Madras, G. (2004). Synthesis and structure of nanocrystalline TiO2 with lower band gap showing high photocatalytic activity. *Langmuir*, 20(7), 2900-2907.
12. Nandiyanto, A.B.D.; Iskandar, F.; and Okuyama, K. (2009). Macroporous anatase titania particle: Aerosol self-assembly fabrication with photocatalytic performance. *Chemical Engineering Journal*, 152(1), 293-296.
13. Nandiyanto, A.B.D.; Oktiani, R.; Ragadhita, R.; Sukmafitri, A.; and Zaen, R. (2020). Amorphous content on the photocatalytic performance of micrometer-sized tungsten trioxide particles. *Arabian Journal of Chemistry*, 13(1), 2912-2924.
14. Nandiyanto, A.B.D.; Zaen, R.; and Oktiani, R. (2020). Correlation between crystallite size and photocatalytic performance of micrometer-sized monoclinic WO3 particles. *Arabian Journal of Chemistry*, 13(1), 1283-1296.
15. Arutanti, O.; Nandiyanto, A.B.D.; Ogi, T.; Kim, T.O.; and Okuyama, K. (2015). Influences of porous structurization and Pt addition on the improvement of photocatalytic performance of WO3 particles. *ACS Applied Materials and Interfaces*, 7(5), 3009-3017.
16. Ohtani, B.; Ogawa, Y.; and Nishimoto, S.-i. (1997). Photocatalytic activity of amorphous− anatase mixture of titanium (IV) oxide particles suspended in aqueous solutions. *The Journal of Physical Chemistry B*, 101(19), 3746-3752.
17. Tanaka, K.; Capule, M.F.; and Hisanaga, T. (1991). Effect of crystallinity of TiO2 on its photocatalytic action. *Chemical Physics Letters*, 187(1-2), 73-76.
18. Arias, L.F.; Duran, A.A.; Cardona, D.; Camps, E.; Gómez, M.; and Zambrano, G. (2015). Effect of annealing treatment on the photocatalytic activity of TiO2 thin films deposited by dc reactive magnetron sputtering. *Journal of Physics: Conference Series*, 614(1), 012008.
19. Kim, D.S.; and Kwak, S.-Y. (2007). The hydrothermal synthesis of mesoporous TiO_2 with high crystallinity, thermal stability, large surface area, and enhanced photocatalytic activity. *Applied Catalysis A: General*, 323, 110-118.
20. Marotti, R.; Giorgi, P.; Machado, G.; and Dalchiele, E. (2006). Crystallite size dependence of band gap energy for electrodeposited ZnO grown at different temperatures. *Solar Energy Materials and Solar Cells*, 90(15), 2356-2361.
21. Peiró, A.M.; Peral, J.; Domingo, C.; Domènech, X.; and Ayllón, J.A. (2001). Low-temperature deposition of TiO2 thin films with photocatalytic activity from colloidal anatase aqueous solutions. *Chemistry of Materials*, 13(8), 2567-2573.
22. Nandiyanto, A.B.D.; Arutanti, O.; Ogi, T.; Iskandar, F.; Kim, T.O.; and Okuyama, K. (2013). Synthesis of spherical macroporous WO3 particles and their high photocatalytic performance. *Chemical Engineering Science*, 101, 523-532.
23. Nandiyanto, A.B.D. (2019). Hydrothermal synthesis method for the production of nanorod tungsten trioxide particles. *Journal of Engineering Science and Technology*, 14(6), 3105-3113.

24. Andral, M.; Roger, S.; Montrejaud‐Vignoles, M.; and Herremans, L. (1999). Particle size distribution and hydrodynamic characteristics of solid matter carried by runoff from motorways. *Water Environment Research*, 71(4), 398-407.
25. Nandiyanto, A.B.D.; Kim, S.-G.; Iskandar, F.; and Okuyama, K. (2009). Synthesis of spherical mesoporous silica nanoparticles with nanometer-size controllable pores and outer diameters. *Microporous and Mesoporous Materials*, 120(3), 447-453.
26. Nandiyanto, A.B.D.; Andika, R.; Aziz, M.; and Riza, L.S. (2018). Working volume and milling time on the product size/morphology, product yield, and electricity consumption in the ball-milling process of organic material. *Indonesian Journal of Science and Technology*, 3(2), 82-94.
27. Nandiyanto, A.B.D.; Zaen, R.; and Oktiani, R. (2018). Working volume in high-energy ball-milling process on breakage characteristics and adsorption performance of rice straw ash. *Arabian Journal for Science and Engineering*, 43(11), 6057-6066.
28. Borhade, A.V.; and Baste, Y.R. (2017). Study of photocatalytic asset of the ZnSnO3 synthesized by green chemistry. *Arabian Journal of Chemistry*, 10, S404-S411.
29. Nandiyanto, A.B.D. (2017). Mathematical approximation based on thermal analysis curves for calculating kinetic parameters of thermal decomposition of material. *Journal of Engineering Science and Technology*, 12, 76-90.
30. Nandiyanto, A.B.D.; Munawaroh, H.S.H.; Kurniawan, T.; and Mudzakir, A. (2016). Influences of temperature on the conversion of ammonium tungstate pentahydrate to tungsten oxide particles with controllable sizes, crystallinities, and physical properties. *Indonesian Journal of Chemistry*, 16(2), 124-129.
31. Al-Othman, Z.A. (2012). A review: fundamental aspects of silicate mesoporous materials. *Materials*, 5(12), 2874-2902.
32. De Wijs, G.; and De Groot, R. (1999). Structure and electronic properties of amorphous WO3. *Physical Review B*, 60(24), 16463.